Percolation for a model of statistically inhomogeneous random media

J. Quintanilla[a)]
Department of Mathematics, University of North Texas, Denton, Texas 76203

S. Torquato[b)]
School of Mathematics, Institute for Advanced Study, Princeton, New Jersey 08540

(Received 17 May 1999; accepted 8 July 1999)

We study clustering and percolation phenomena for a model of statistically inhomogeneous two-phase random media, including functionally graded materials. This model consists of inhomogeneous fully penetrable (Poisson distributed) disks and can be constructed for any specified variation of volume fraction. We quantify the transition zone in the model, defined by the frontier of the cluster of disks which are connected to the disk-covered portion of the model, by defining the coastline function and correlation functions for the coastline. We find that the behavior of these functions becomes largely independent of the specific choice of grade in volume fraction as the separation of length scales becomes large. We also show that the correlation function behaves in a manner similar to that of fractal Brownian motion. Finally, we study fractal characteristics of the frontier itself and compare to similar properties for two-dimensional percolation on a lattice. In particular, we show that the average location of the frontier appears to be related to the percolation threshold for homogeneous fully penetrable disks. © *1999 American Institute of Physics.* [S0021-9606(99)51037-4]

I. INTRODUCTION

Much progress has been made in recent years in characterizing the microstructure of statistically homogeneous two-phase random media. This microstructural information in turn has been used to rigorously determine the effective macroscopic properties of such media.[1–8] However, significantly less research has been devoted to the study of *statistically inhomogeneous* two-phase media, including porous media with spatially variable fluid permeability,[9] distributions of galaxies,[10] and functionally graded materials.[11–15] For such media, ergodicity is lost; that is, one cannot equate ensemble and volume averages, and the volume fraction is position dependent.

Following the development of the study of the microstructure and properties of homogeneous random media,[1] the authors have proposed a microstructural model for particulate, statistically inhomogeneous two-phase random media.[16] This model is a two-phase system consisting of an inhomogeneous distribution of fully penetrable spheres in space whose particle density obeys any specified variation in volume fraction. The space exterior to the spheres is called phase 1, and phase 2 is the space occupied by the spheres. The authors have analytically obtained certain *n*-point correlation functions for this model,[16] which will undoubtedly be fundamental in the study of the effective properties of statistically inhomogeneous random media.

This inhomogeneous model is nontrivial in that cluster formation naturally arises and it permits more complicated microstructures than, for example, layered models of statistically inhomogeneous random media[17] and lattice models of gradient percolation.[18] For instance, consider the system of inhomogeneous fully penetrable disks as depicted in Fig. 1. The length scale of the system is chosen to be 100 times larger than the radii of the disks, while the grade in the volume fraction of phase 2 is prescribed to be

$$\phi_2(x)=x; \tag{1}$$

in other words, the system has a linear grade in volume fraction. The disks that are connected to the right-hand edge are shown in black, while the disks that are not connected are only outlined. We observe that the right-hand edge is covered by disks, while the left-hand edge has no disks. In between, there is a ''transition zone'' in which the disks are no longer connected to the disks on the right-hand edge. Following Sapoval, Rosso, and Gouyet,[19] we define the edge of the connected cluster to be the *frontier*; this is shown with the thick black line in Fig. 1. The fractal properties of this transition zone have been studied for gradient percolation on the lattice;[18,19] characterizing this region for inhomogeneous fully penetrable disks is the focus of this paper.

We will consider a model of inhomogeneous continuum percolation in the unit square. Specifically, we will consider systems of inhomogeneous fully penetrable disks with a grade in volume fraction dependent only on the x-coordinate so that $\phi_2(0)=0$, $\phi_2(1)=1$, and $\phi_2'(x)>0$ for $0<x<1$. Although higher dimensional systems can also be treated, we do not do so in this paper. In Sec. II, to study the transition zone, we define the *coastline function* for these systems. In Sec. III, we will study the values of the coastline function and their dependence upon the separation of length scales. In

a)Electronic mail: johnq@unt.edu
b)Author to whom correspondence should be addressed. Electronic mail: torquato@matter.princeton.edu. On sabbatical leave. Permanent address: Princeton Materials Institute, Princeton University, Princeton, New Jersey 08544.

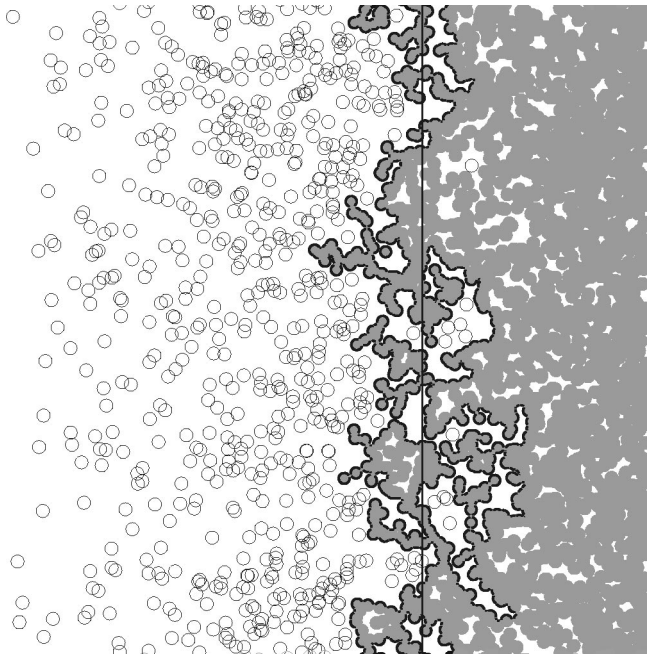

FIG. 1. A realization of inhomogeneous fully penetrable disks. The system size is 100 times larger than the radii of the disks, so that $\ell = 100$. We see the presence of a ''transition zone'' in which the disks are no longer connected to the right-hand edge. The frontier is outlined in black. The average position of the frontier, determined by Eq. (20), is indicated by the thin vertical line.

Sec. IV, we will study correlation functions of the coastline. We show that, as the separation of length scales becomes large, the behavior of the coastline is largely independent of the specific choice of grade in volume fraction. We also show that the correlation function behaves in a manner similar to that of fractal Brownian motion. Finally, in Sec. V, we will study the fractal properties of the frontier itself and compare them with analogous results for gradient percolation on a two-dimensional lattice. We also conjecture that the average position of the frontier is related to the percolation threshold of homogeneous fully penetrable disks.

II. CHARACTERIZATION AND SIMULATION OF THE TRANSITION ZONE

To simulate a system of homogeneous fully penetrable disks, both the density ρ of particles per unit area and the radius R of the disks must be specified. The model is then formed by centering disks of radius R on the points of a Poisson process with density ρ. By contrast, for *inhomogeneous* fully penetrable disks, the underlying particle density is a function $\rho(\mathbf{x})$ of the position within the model. The volume fraction $\phi_2(\mathbf{x})$ is then related to the density function $\rho(\mathbf{x})$ by[16]

$$\phi_2(\mathbf{x}) = 1 - \exp\left[- \int_B \rho(\mathbf{y}) d\mathbf{y} \right], \tag{2}$$

where B is the disk of radius R centered at $\mathbf{x}$. Assuming that the length scale of ρ is much larger than the radii of the disks, we can accurately approximate the grade in volume fraction by

$$\phi_2(\mathbf{x}) = 1 - e^{-\pi R^2 \rho(\mathbf{x})}. \tag{3}$$

Constructing realizations of inhomogeneous fully penetrable disks can be easily done in two stages if the density function $\rho(\mathbf{x})$ is bounded,[20] say, $\rho(\mathbf{x}) \leqslant \rho^*$. First, an ordinary Poisson process with density ρ^* is simulated. Each point $\mathbf{x}$ of the Poisson process, independently of the other points, is then kept with probability $\rho(\mathbf{x})/\rho^*$ or deleted with probability $1 - \rho(\mathbf{x})/\rho^*$. The resulting point pattern is a general Poisson process with density function $\rho(\mathbf{x})$. A system of fully penetrable disks is then obtained by centering disks of fixed radius R upon the points of this general Poisson process.

We now consider the simulation of the frontier and the coastline function. The grades in volume fraction considered in this paper are dependent on only the x-coordinate so that $\phi_2(x)$ increases from 0% to near 100% as x moves from the left edge to the right edge. We use a standard burning algorithm to determine which disks are in the same cluster as the particles on the right-edge; we call this group of particles the *percolating cluster*. While we permit periodic boundary conditions along the top and bottom edges, we do not do so for the left and right edges. This type of percolation is different than percolation for statistically homogeneous random media, since, for a large separation of length scales, the probability that this cluster extends to the left edge is negligible.

In practice, for computational efficiency, we only simulate the portion of a system for which the volume fraction lies between two prescribed values, that is,

$$\phi_2^{\min} \leqslant \phi_2(x) \leqslant \phi_2^{\max}. \tag{4}$$

The separation of length scales is then defined by

$$\ell = [R(\phi_2^{\max} - \phi_2^{\min})]^{-1}. \tag{5}$$

Recall that the square containing the particles is given unit length.

In order to determine the percolating cluster, all groups of disks connected to the right edge where $\phi_2 = \phi_2^{\max}$ are identified. There may be multiple such groups, since, for example, it is possible for a single particle along the right edge to be unconnected to any other disks and hence form a group by itself. While multiple groups are possible, in practice, most groups will be insignificant in size compared with one very large group. We identify the percolating cluster to be the group of disks which extends the furthest left; that is, the group that contains the disk which both is connected to the right edge and has the smallest value of $\phi_2(x)$.

We define the *frontier* to be the set of arcs on the boundary of the percolating cluster. We notice in Fig. 1 that the frontier is not the graph of a function of y; there may be several points on the frontier at any given y-coordinate. For each y-coordinate in a given realization, we define the *height* $h(y)$ to be the value of ϕ_2 which corresponds to the smallest (leftmost) x-coordinate so that (x,y) belongs to the percolating cluster. We will often refer to all such points (x,y) as the *coastline* for a given realization. We see that the coastline is the graph of a *single-valued* function of the y-coordinates, while the entire frontier represents a multivalued function. The coastline is thus defined as a subset of the frontier; in fact, an arc in the frontier may only be partially contained in

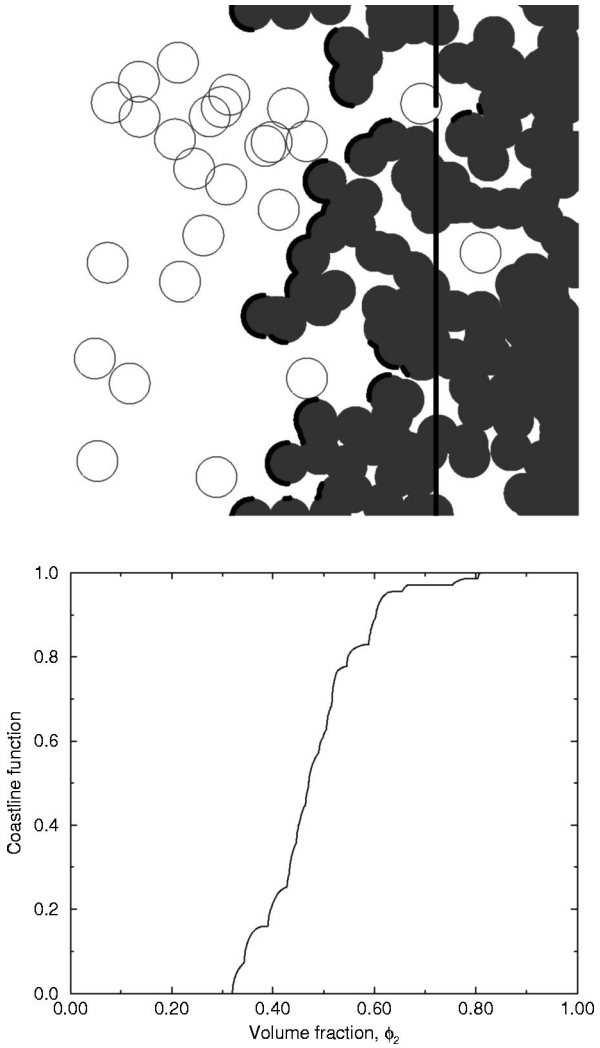

FIG. 2. The coastline and coastline function for one realization of fully penetrable disks for which $\ell = 25$. The coastline is defined as the leftmost arcs of the frontier. The coastline function at ϕ is defined to be the fraction of y-coordinates for which the height function is less than ϕ. For any one realization, the graph of the coastline function will have multiple corners.

the coastline. Simulation of the coastline thus requires some meticulous record-keeping since only the leftmost portions of the frontier are stored.

We finally define the *coastline function* $c(\phi_2)$ to be

$$c(\phi_2) = \Pr(h(y) \leqslant \phi_2). \tag{6}$$

In a simulation, this probability is empirically measured as the fraction of y-coordinates for which the height function is less than or equal to ϕ_2. This fraction is measured exactly for each realization.

For any one realization, the height and coastline functions can be rather choppy, as illustrated in Fig. 2. In this figure, the coastline function for one realization of fully penetrable disks for $\ell = 25$ is shown. We see that there are many corners in the graph of the coastline function as ϕ_2 and c increase from 0 to 1. For this particular realization, there is a small region in which c is constant at approximately 98%; this corresponds to the values of ϕ_2 in the realization (represented by the vertical line) which are not assumed by the height function. In this realization, for approximately 98% of

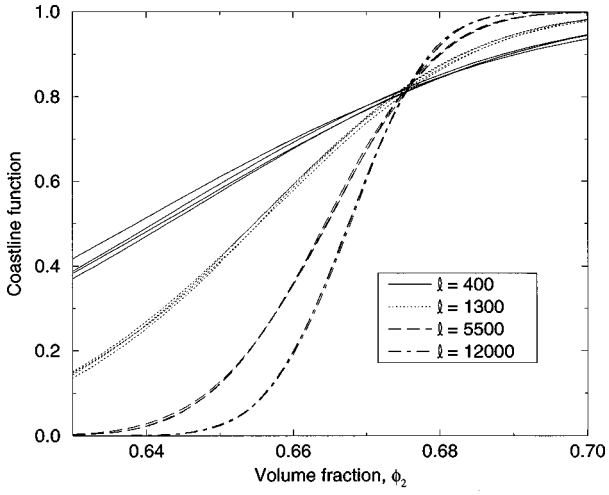

FIG. 3. Graphs of the coastline function for systems of fully penetrable disks at $\ell = 400$, 1300, 5500, and 12000. The grades in volume fraction of Eqs. (7)–(10) are simulated for each of these values of ℓ. The coastline tends to be more vertical—concentrated over a smaller range of volume fractions—as the separation in length scales increases. We also see that the behavior of the coastline function is almost invariant under the choice of the grade in volume fraction.

the coordinates on the vertical line, the coastline is to the left of the line. In order to smooth out these corners, the coastline function is obtained by averaging the values of the height function over thousands of realizations.

In the next two sections, we consider properties of the coastline function; we consider the fractal characteristics of the entire frontier in Sec. V.

III. VALUES OF THE COASTLINE FUNCTION

In Fig. 3, we present graphs of the coastline function for systems of fully penetrable disks when ℓ, the separation of length scales, is 400, 1300, 5500, and 12000. We see that the coastline becomes more vertical as ℓ increases. That is, the range of values of the height function narrows as the separation of length scales increases. For example, nearly half of the coastline extends to the $\phi_2 \leqslant 0.64$ portion of the system when $\ell = 400$. At $\ell = 1300$, about one-fifth of the coastline lies in this part of the system. A much smaller portion of the coastline is in this regime when $\ell = 5500$, while the coastline almost never extends to this part of the system when $\ell = 12000$.

By way of comparison, the percolation threshold for statistically homogeneous fully penetrable disks is known from simulations to be approximately 67.6%.[21–23] It appears that the support of the coastline function converges to approximately this value as ℓ increases. This convergence will be discussed in greater detail in Sec. V. It is not surprising that the convergence comes from below; the height function $h(y)$ is defined to be the least x-coordinate on the frontier associated with a given y.

Four different grades in volume fraction were chosen for simulation:

$$\phi_2(x) = x\phi_2^{\max} + (1-x)\phi_2^{\min}, \tag{7}$$

$$\phi_2(x) = 1 - [x\sqrt{\phi_1^{\min}} + (1-x)\sqrt{\phi_1^{\max}}]^2, \tag{8}$$

$$\phi_2(x) = [x\sqrt{\phi_2^{\max}} + (1-x)\sqrt{\phi_2^{\min}}]^2, \tag{9}$$

$$\phi_2(x) = 1 - \phi_1^{\max}\left(\frac{\phi_1^{\min}}{\phi_1^{\max}}\right)^x. \tag{10}$$

In these equations, $\phi_1^{\min} = 1 - \phi_2^{\max}$ and $\phi_1^{\max} = 1 - \phi_2^{\min}$ are the minimum and maximum values of the matrix phase (phase 1) in a given simulation. The first equation is a linear grade in volume fraction, the next two are quadratic grades, and the last is an exponential grade in volume fraction. All four grades are parameterized so that $\phi_2(0) = \phi_2^{\min}$ and $\phi_2(1) = \phi_2^{\max}$.

The graphs of the coastline function for each of these grades are plotted in Fig. 3. For $\ell = 400$, we see that the choice in grade makes a significant difference in the behavior of c. For $\ell = 1300$, the behavior of the graphs of c are more similar. Even this small difference virtually vanishes on the scale of the figure when ℓ is either 5500 or 12000. We conclude that the behavior of the coastline function is largely independent of the choice of $\phi_2(x)$ when ℓ is sufficiently large. That is, the coastline extends to the same region of ϕ_2 for these different systems, although the percolating cluster will extend to different x-coordinates.

This observation is physically reasonable. Systems of statistically inhomogeneous fully penetrable disks are described by two length scales; ℓ, relating the size of the square to the size of the disks, and the length scale of the grade in volume fraction. We expect that the parameter ℓ to dominate the behavior of the entire system and hence the coastline as ℓ becomes large.

We also notice a very surprising result from our simulations: regardless of the grade in volume fraction or the separation of length scales, the graph of the coastline function appears to be roughly 0.8 when $\phi_2 = 0.676$. In other words, for all of these graphs, about 80% of the coastline (a majority of the frontier's leftmost arcs) lie to the left of the critical point.

IV. CORRELATION FUNCTIONS OF THE HEIGHT FUNCTION

The final statistical characterizations of the coastline considered in this report are certain correlation functions of the height function. One such characterization, which has been studied and measured extensively in the literature, is the height-height correlation function $\langle w^2(z)\rangle$, where

$$w(z) = h(y) - h(y+z). \tag{11}$$

Since h is stationary, $\langle w^2(z)\rangle$ is independent of y.

In the literature, the methods of fractal Brownian motion[24,25] have been used to characterize the behavior of this correlation function. A fractal Brownian motion $X(z)$ is a stochastic process whose two-point correlation function obeys the relation

$$\langle X(z)X(z')\rangle \propto |z-z'|^{2H}, \tag{12}$$

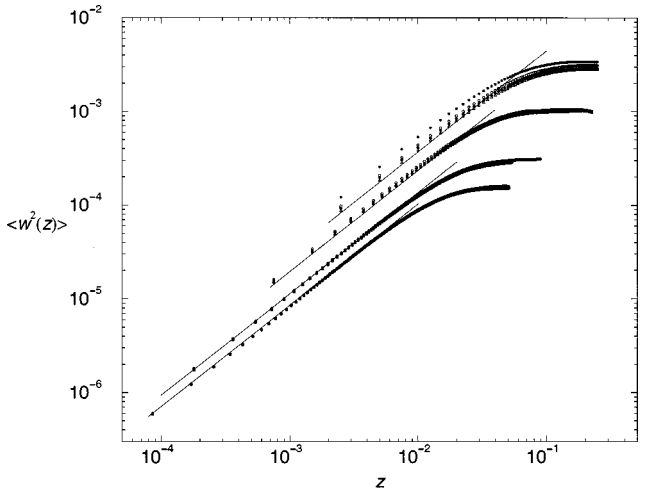

FIG. 4. Log–log graphs of the height-height correlation function $\langle w^2\rangle$ at (from top to bottom) $\ell = 400$, 1300, 5500, and 12000. The four grades in volume fraction are simulated for each value of ℓ; filled circles for Eq. (7), open circles for Eq. (8), triangles for Eq. (9), and stars for Eq. (10). The lines, given by Eq. (13), are approximations to the slanted linear portions of these graphs.

where $0 < H \leqslant 1$. If $H = \frac{1}{2}$, then the process X obeys ordinary Brownian motion.

In Fig. 4, we have plotted, on a log–log graph, simulations of $\langle w^2\rangle$ for the four different grades in volume fraction of Eqs. (7)–(10). In this figure, from top to bottom, are the graphs of $\langle w^2\rangle$ for $\ell = 400$, 1300, 5500, and 12000. The abscissa represents z, the distance between y-coordinates in the system, as a fraction of the side length of the system. Each set of graphs has the same qualitative behavior; the graphs have a slanted linear portion which eventually plateaus for sufficiently large z. We see that the behavior of this correlation function is sensitive to the choice of grade for small values of ℓ. However, the choice of grade becomes less influential as ℓ increases.

The straight lines in Fig. 4 are empirical approximations to the slanted linear portions of the graphs. We find that

$$\ln\langle w^2\rangle \approx -0.653 - 0.4 \ln \ell + 1.08 \ln z, \tag{13}$$

or

$$\langle w^2\rangle \approx 0.52\ell^{-0.4} z^{1.08} \tag{14}$$

for sufficiently small values of z. In Fig. 5, we have rescaled the axes and redrawn the four graphs for $\ell = 5500$ and $\ell = 12000$. We see that these graphs collapse onto a single graph, following a scaling law of the form

$$\langle w^2\rangle \ell^{0.864} \approx 0.52(z\ell^{0.43})^{1.08} \tag{15}$$

for sufficiently small values of z. This behavior has been similarly observed in the linear portion of $\langle w^2\rangle$ in other studies on rough interfaces.[24,25] The exponents 0.43 and 0.864 are related to the exponent of Eq. (18) below.

Finally, the autocorrelation function of the height function is defined to be

$$C(z) = \frac{\langle [h(y) - p_h][h(y+z) - p_h]\rangle}{\sigma_h^2}, \tag{16}$$

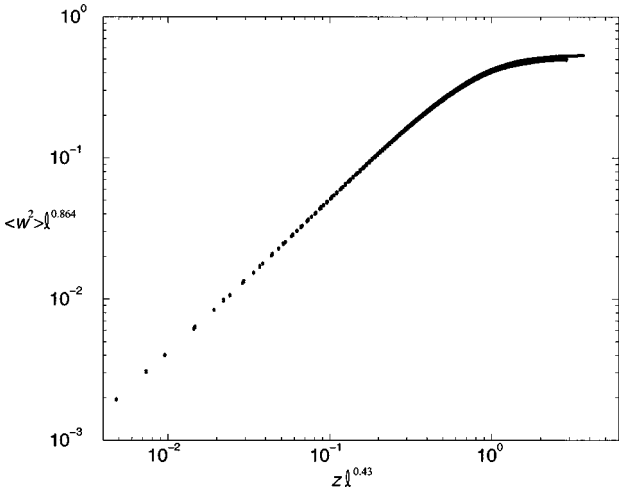

FIG. 5. The graphs in Fig. 4 for $\ell=5500$ and $\ell=12000$, but rescaled with axes $z\ell^{0.43}$ and $\langle w^2\rangle l^{0.864}$. Notice that all eight graphs collapse to a single curve.

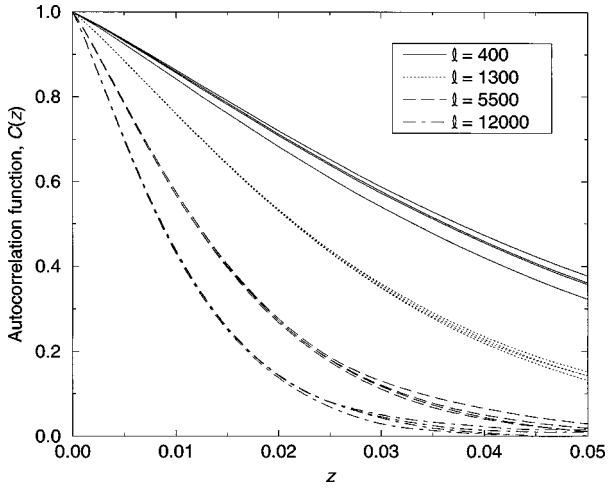

FIG. 6. Graphs of the autocorrelation function for systems of fully penetrable disks at $\ell=400$, 1300, 5500, and 12000. The absicca represents the distance between y-coordinates in the system as a fraction of the side length of the system. We see that the correlation length of the coastline decreases significantly as the separation in length scales increases. We also see that the autocorrelation function $C(z)$ is somewhat more sensitive to the grade in volume fraction for large values of z.

where p_h and σ_h are the mean and standard deviation of the height function $h(y)$; these are measured from the simulations. Again, $C(z)$ is independent of y. By construction, $|C(z)|\leqslant 1$ and $C(0)=1$. If $|C(z)|\approx 1$, then $h(y)$ is an excellent predictor of the value of $h(y+z)$. On the other hand, if $C(z)\approx 0$, then the values of $h(y)$ and $h(y+z)$ are essentially uncorrelated. The autocorrelation function is related to the height–height correlation function through the equation

$$\langle w^2(z)\rangle = 2\sigma_h^2[1-C(z)]. \tag{17}$$

In Table I, we give the observed values of p_h and σ_h in our computer simulations. We see that σ_h decreases (in other words, the range of possible values for the height function narrows) as the separation of length scales increases. From this data and from additional simulations with intermediate values of ℓ, we find that

$$\sigma_h \approx 0.5\ell^{-0.432} \tag{18}$$

is an excellent empirical approximation for σ_h. The uncertainties in the values of p_h and σ_h are caused by the four choices of grade in volume fraction as well as the random fluctuations inherent in the simulation. We conclude again that the choice of grade in volume fraction does not greatly affect the behavior of the coastline for large values of ℓ. We note that this exponent is approximately $-3/7$; this will be discussed in Sec. V.

In Fig. 6, we present graphs of the autocorrelation function for systems of fully penetrable disks at $\ell=400$, 1300, 5500, and 12000. The four different grades in volume fraction were again simulated at each value of ℓ. We see that the correlation length of the coastline decreases significantly as the separation in length scales increases. We also see that the autocorrelation function $C(z)$ is more sensitive to the choice of grade in volume fraction than the values of the coastline function. This sensitivity becomes more prominent for large values of z. However, the specific choice of grade in volume fraction again becomes unimportant as ℓ becomes large.

In Fig. 7, we have rescaled the axes and redrawn the four

TABLE I. The observed means and standard deviations of the height function for various values of ℓ. The errors in the values of p_h and σ_h are caused by the four different grades in volume fraction selected as well as the inherent random fluctuations in the computer simulations. We see that the choice of grade in volume fraction causes less uncertainty in the values of p_h and σ_h as ℓ increases. We also observe that σ decreases (that is, the range of values that the height function assumes becomes narrower) as the separation in length scales increases. As expected, p_h for the coastline approaches the percolation threshold for homogeneous fully penetrable disks as ℓ increases.

ℓ	400	1300	5500	12000
p_h	0.6397 ± 0.0019	0.6544 ± 0.0003	0.6642 ± 0.0001	0.6676 ± 0.0001
σ_h	0.0395 ± 0.0016	0.0225 ± 0.0003	0.0121 ± 0.0001	0.0088 ± 0.0001

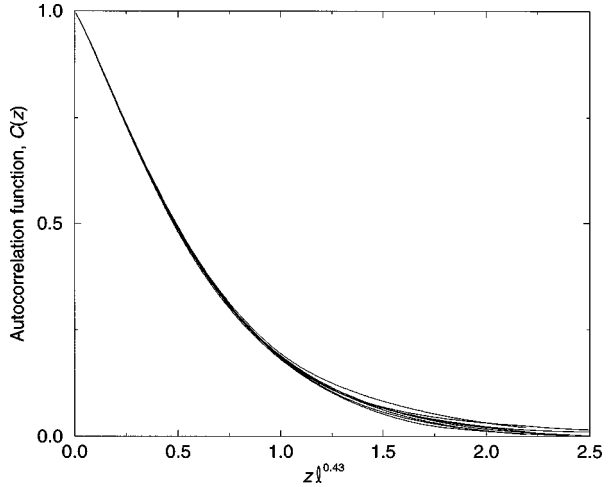

FIG. 7. The graphs in Fig. 6 for $\ell=5500$ and $\ell=12000$, but rescaled with axes $z\ell^{0.43}$ and $C(z)$. Notice that all eight graphs collapse to a single curve for even moderate values of z.

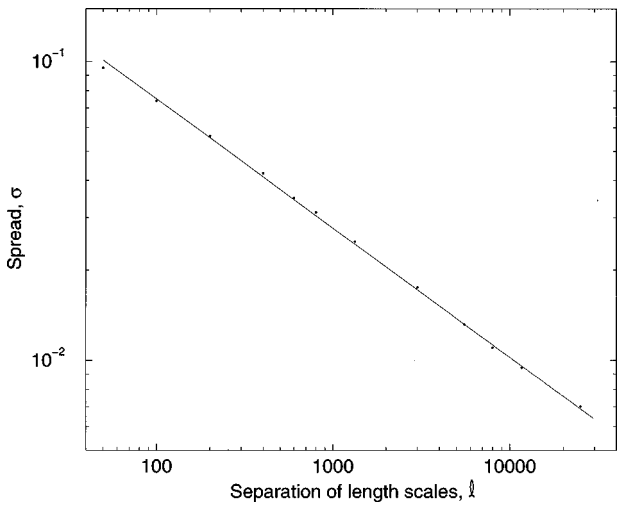

FIG. 8. A graph of the spread σ of the frontier as a function of ℓ. The observed data are given by dots, and a regression fit has been used to fit the data. The equation of this fit to the data is given by Eq. (24). Similar behavior has been observed in site percolation on a square lattice and indicates a universal feature of two-dimensional percolation.

graphs for $\ell=5500$ and $\ell=12000$. We see that these eight graphs collapse to a single curve, similar to Fig. 7.

V. FRACTAL PROPERTIES OF THE FRONTIER

A. Simulating and characterizing the frontier

The frontier of the percolating cluster is not a function of the y-coordinates. In the previous sections, we defined the height function, whose graph is a subset of the frontier, and subsequently defined the coastline function. In this section, we study the fractal properties of the entire frontier. In particular, we measure the perimeter of the frontier, its average position, and its width and consider its fractal properties.

The simulation of the frontier is somewhat easier than the prior simulations of the height and coastline functions. In the previous sections, great care was needed to ensure that only the leftmost arcs of the frontier were stored; dropping this restriction considerably simplifies the simulation. Determining the frontier thus reduces to finding the points of intersection of the disks on the boundary. For each arc i on the frontier, we store the center (x_i,y_i) of its disk and the minimum and maximum angles α_i and β_i which bound the arc. This simulation was first performed by Rosso.[22]

In the previous sections, we noticed how little the specific choice of $\phi_2(x)$ influenced the behavior of the coastline function. Accordingly, we only choose a linear grade in the volume fraction of the disks, given by Eq. (7), to study the frontier. We also perform this simulation over a wider range of separation of length scales, with ℓ varying from 50 to 25000.

For a given realization, the perimeter of the frontier is easily measured as

$$P=\sum R(\beta_i-\alpha_i). \tag{19}$$

We recall that the simulation is taken in a square of unit length, thus standardizing P for all values of ℓ.

To measure the average position $\overline{x}$ of the frontier, we empirically calculate the expected value (averaged over arc length) of the x-coordinates of the frontier. This yields the expression

$$\overline{x}=\frac{R}{P}\sum\int_{\alpha_i}^{\beta_i}(x_i+R\cos\theta)d\theta$$

$$=\frac{R}{P}\sum[x_i(\beta_i-\alpha_i)+R(\sin\beta_i-\sin\alpha_i)]. \tag{20}$$

In Fig. 1, this average position is depicted by the thin vertical line through the frontier. To standardize the results for different values of ℓ, we then calculate

$$p=\phi_2(\overline{x}), \tag{21}$$

the volume fraction of disks at $\overline{x}$.

To measure the spread of the frontier about this average position, we calculate the standard deviation of the $x-$coordinates. For a given realization, this is obtained from

$$\sigma_x^2=\left[\frac{R}{P}\sum\int_{\alpha_i}^{\beta_i}(x_i+R\cos\theta)^2d\theta\right]-\overline{x^2}$$

$$=\frac{R}{P}\sum\left[\left(x_i^2+\frac{R^2}{2}\right)(\beta_i-\alpha_i)+2Rx_i(\sin\beta_i-\sin\alpha_i)\right.$$

$$\left.+\frac{R^2}{4}(\sin 2\beta_i-\sin 2\alpha_i)\right]-\overline{x^2}. \tag{22}$$

Again, to standardize results for different values of ℓ, we then calculate

$$\sigma=\phi_2(\overline{x})-\phi_2(\overline{x}-\sigma_x), \tag{23}$$

thus expressing the spread in terms of the grade in volume fraction. This conversion is permitted since we are now considering only a linear grade in volume fraction.

The above formulas are valid for one realization. These sample values are then averaged over thousands of realizations to obtain our estimates of P, p, and σ. In this study, we used enough realizations to determine p with an error of less than 5×10^{-5}; the exact number of realizations depended on the choice of ℓ.

B. Results and analysis

In Fig. 8, we present a graph of the spread σ as a function of the separation of length scales ℓ. It is apparent from the graph that σ exhibits power-law behavior. Using the values for $\ell\geqslant800$, we find that

$$\sigma\propto\ell^{-0.432}. \tag{24}$$

Comparison with previous research suggests that this may be a universal feature of two-dimensional percolation. The fractal dimension of the percolating hull of two-dimensional percolation on a lattice has been shown to be equal to 7/4,[26] and it is conjectured that this is also the fractal dimension of the frontier for gradient percolation on a lattice.[19] Therefore, according to the scaling theory of Sapoval, Rosso, and Gouyet,[19]

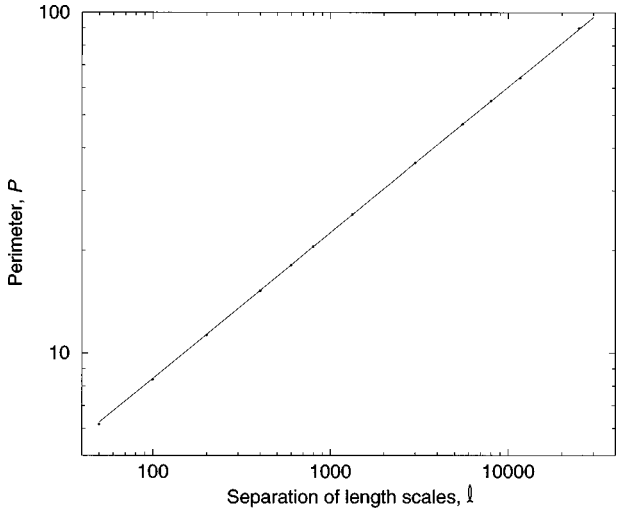

FIG. 9. A graph of the scaled perimeter P of the frontier as a function of ℓ. The observed data are given by dots, and a regression fit has been used to fit the data. The equation of this fit to the data are given by Eq. (26). Similar behavior has been observed in site percolation on a square lattice and indicates a universal feature of two-dimensional percolation.

$$\sigma_x \propto \ell^{4/7} \tag{25}$$

for gradient percolation on a lattice. (We have written this equation using our notation.) This exponent was found by simulations for a square lattice with linear[18] and nonlinear[19] grades in occupation probability. The exponent is close to that of Eq. (24) since $\sigma_x \propto \ell\sigma$. We also note that the exponent in Eq. (24) is, not surprisingly, the same as the exponent in Eq. (18) to three decimal places.

In Fig. 9, we present a graph of the perimeter P as a function of ℓ. Again using the data for $\ell \geqslant 800$, we find that

$$P \propto \ell^{0.428}. \tag{26}$$

We observe that this power-law behavior is approximately correct even for $\ell = 50$. The exponent found for a nonlinear grade on a square lattice was 3/7,[19] indicating that this too may be a universal feature of two-dimensional gradient percolation.

In Fig. 10, we present p as a function of $1/\ell$. We see that the observed values of p appear vary linearly with $1/\ell$. (As an aside, the values of p_h—the average location of the coastline from Sec. IV—do not appear to vary linearly with $1/\ell$.) Following similar results for two-dimensional lattice percolation,[18,27] we conjecture that as $\ell \to \infty$, p converges to the ordinary percolation threshold of *homogeneous* fully penetrable disks. Using a regression fit for the data corresponding to $\ell \geqslant 800$, we estimate (to one standard deviation) the percolation threshold for a continuum model of fully penetrable disks as

$$p_c = 0.67637 \pm 0.00005. \tag{27}$$

This is in agreement with previous estimates of the percolation threshold,[22,23] although an extra decimal place of accuracy has been added in our study. On lattices, the numerical evidence for a similar connection between gradient percolation and ordinary percolation is quite compelling. However, a formal proof of such a connection has yet to be discovered.

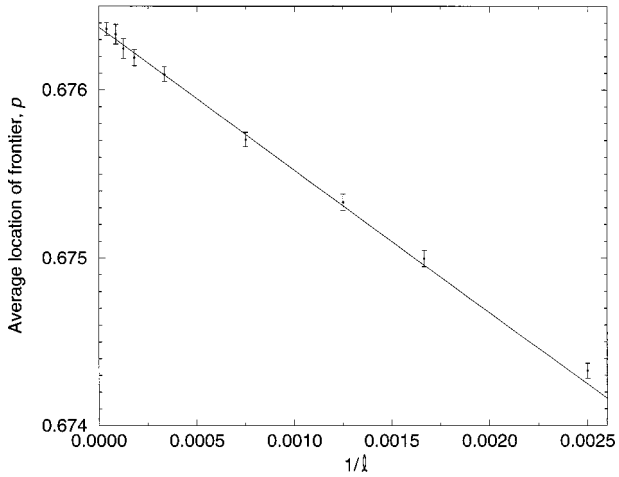

FIG. 10. A graph of the average location of the frontier $p = \phi_2(\overline{x})$ as a function of $1/\ell$. The observed data are given by dots, and a regression fit has been used to fit the data. We conjecture in Eq. (27) that, as $\ell \to \infty$, p converges to the percolation threshold of homogeneous fully penetrable disks.

VI. CONCLUSIONS

In order to quantify percolation for statistically inhomogeneous fully penetrable disks, we have defined the coastline function and the correlation functions for the height function. We have used computer simulations to measure these functions under a variety of grades in volume fraction and also separations of length scales. We have found that the specific choice of grade in volume fraction does not greatly affect the behavior of these functions as the separation in length scales becomes large. We have also found that the height–height correlation function has the same form as that of fractal Brownian motion for a fixed value of the separation of length scales. Finally, we have calculated fractal properties of the entire coastline and have observed a strong connection between lattice and continuum gradient percolation. We have also conjectured a relationship between the percolation phenomena of the present model and of the archetypal model of two-dimensional continuum percolation, fully penetrable disks on the plane.

ACKNOWLEDGMENTS

The authors thank R. M. Ziff for many helpful comments. S.T. gratefully acknowledges the support of the Engineering Research Program Office of Basic Energy Sciences at the Department of Energy under Grant No. DE-FG02-92ER14275.

[1] S. Torquato, Appl. Mech. Rev. **44**, 37 (1991).
[2] H. L. Weissberg and S. Prager, Phys. Fluids **13**, 2958 (1970).
[3] M. Doi, J. Phys. Soc. Jpn. **40**, 567 (1976).
[4] G. W. Milton, Phys. Rev. Lett. **46**, 542 (1981).
[5] G. W. Milton and N. Phan-Thien, Proc. R. Soc. London, Ser. A **380**, 305 (1982).
[6] A. K. Sen and S. Torquato, Phys. Rev. B **39**, 4504 (1989).
[7] J. Quintanilla and S. Torquato, J. Appl. Phys. **77**, 4361 (1995).
[8] J. Quintanilla, Polym. Eng. Sci. **39**, 559 (1999).
[9] L. W. Gelhar, *Stochastic Subsurface Hydrology* (Prentice–Hall, Englewood Cliffs, 1993).
[10] J. R. Bond, L. Kofman, and D. Pogosyan, Nature (London) **380**, 603 (1996).

[11] J. Aboudi, S. M. Arnold, and M.-J. Pindera, Composites Eng. **4**, 1 (1994).
[12] N. Cherradi, A. Kawasaki, and M. Gasik, Composites Eng. **4**, 883 (1994).
[13] G. J. Dvorak and J. Zuiker, in *IUTAM Symposium on Anisotropy, Inhomogeneity, and Nonlinearity in Solid Mechanics*, edited by D. F. Parker and A. H. England (Kluwer Academic, Netherlands, 1995), p. 103.
[14] A. J. Markworth, K. S. Ramesh, and W. P. Parks, Jr., J. Mater. Sci. **30**, 2183 (1995).
[15] J. C. Nadeau and M. Ferrari, Composites Eng. **5**, 821 (1995).
[16] J. Quintanilla and S. Torquato, Phys. Rev. E **55**, 1558 (1997).
[17] T. Reiter, G. J. Dvorak, and V. Tvergaard, J. Mech. Phys. Solids **45**, 1281 (1997).
[18] M. Rosso, J. F. Gouyet, and B. Sapoval, Phys. Rev. B **32**, 6053 (1985).
[19] B. Sapoval, M. Rosso, and J. F. Gouyet, J. Phys. (France) Lett. **46**, L149 (1985).
[20] D. Stoyan, W. S. Kendall, and J. Mecke, *Stochastic Geometry and Its Applications*, 2nd ed. (Wiley, New York, 1995).
[21] S. W. Haan and R. Zwanzig, J. Phys. A **10**, 1547 (1977).
[22] M. Rosso, J. Phys. A **22**, L131 (1989).
[23] B. Lorenz, I. Orgzall, and H.-O. Heuer, J. Phys. A **26**, 4711 (1993).
[24] F. Family and T. Vicsek, *Dynamics of Fractal Surfaces* (World Scientific, Singapore, 1991).
[25] B. J. West and W. Deering, Phys. Rep. **246**, 1 (1994).
[26] H. Saleur and B. Duplantier, Phys. Rev. Lett. **58**, 2325 (1987).
[27] R. M. Ziff and P. N. Suding, J. Phys. A **30**, 5351 (1997).